Constraints on the Efficiency of Electromicrobial Production

Farshid Salimijazi[a], Jaehwan Kim[b,c], Alexa Schmitz[a], Richard Grenville[d], Andrew Bocarsly[b], and Buz Barstow*[a]

[a] *Department of Biological and Environmental Engineering, Cornell University, Ithaca, NY 14853, USA*
[b] *Department of Chemistry, Princeton University, Princeton, NJ 08540, USA*
[c] *Present Address: Department of Chemistry and Chemical Biology, Cornell University, Ithaca, NY 14853, USA*
[d] *Philadelphia Mixing Solutions Ltd., Palmyra, PA 17078, USA*

June 25, 2020

Abstract

Electromicrobial production technologies (EMP) aim to combine renewable electricity and microbial metabolism. We have constructed molecular to reactor scale models of EMP systems using H_2-oxidation and extracellular electron transfer (EET). We predict the electrical-to-biofuel conversion efficiency could rise to $\geq$ 52% with *in vivo* CO_2-fixation. H_2 and EET-mediated EMP both need reactors with high surface areas. H_2-diffusion at ambient pressure requires areas 20 to 2,000 times that of the solar photovoltaic (PV) supplying the system. Agitation can reduce this to less than the PV area, and the power needed becomes negligible when storing $\geq$ 1.1 megawatts. EET-mediated systems can be built that are $\leq$ 10 times the PV area and have minimal resistive energy losses if a conductive extracellular matrix (ECM) with a resistivity and height seen in natural conductive biofilms is used. The system area can be reduced to less than the PV area if the ECM conductivity and height are increased to those of conductive artificial polymers. Schemes that use electrochemical CO_2-fixation could achieve electrical-to-fuel efficiencies of almost 50% with no complications of O_2-sensitivity.

1 Introduction

We are moving towards a world of plentiful renewable electricity [1–3]. However, to enable high penetration of renewables onto the grid, energy storage with a capacity thousands of times greater

*Corresponding author

than today's will be essential [4–7]. Despite significant advances in electrified transportation, the need for hydrocarbons in many applications like aviation could persist and even grow for decades to come [3]. Likewise, the need to sequester tens of gigatonnes of CO_2 per year will also continue to grow [8, 9]. Electromicrobial production (EMP) technologies that combine biological and electronic components have the potential to use renewable electricity to power the capture and sequestration of atmospheric CO_2 and convert it into high-density, non-volatile infrastructure-compatible transportation fuels [7, 10–12].

One of the most successful demonstrations of electromicrobial production to date, the Bionic Leaf [13, 14], is capable of converting solar power to the biofuel isopropanol at efficiencies exceeding the theoretical maximum of C_3 and C_4 photosynthesis [15, 16]. If coupled to some of the most efficient Si or GaAs solar photovoltaics (PVs) [17], the Bionic Leaf could even outperform cyanobacterial photosynthesis, the most efficient form found in nature [18]. However, the energy storage cost of photosynthesis is ultra-low [19, 20]. Any system that aims to supplant photosynthesis will need to dramatically exceed its efficiency, its convenience and preferably both.

To date, no one has systematically explored the constraints on the efficiency of electromicrobial production systems. Here we present a model for comparing the theoretical efficiencies of systems that supply electrons to metabolism by either H_2-oxidation [13, 14, 21, 22] or through a conductive extracellular matrix (ECM) by extracellular electron transfer (EET) [23]; employ *in vivo* enzymatic, or *ex vivo* electrochemical CO_2 fixation [24]; and transform fixed carbon to the biofuels isopropanol [25] or butanol [20–22]. This analysis lets us calculate the maximum theoretical efficiency of each system and gives a roadmap for how to achieve it.

Theory, Results and Discussion

General Theory

Figs. 1A and **1B** show simplified schematics of electromicrobial production systems with *in vivo* and *ex vivo* CO_2-fixation, respectively. In **Fig. 1A** a microbe absorbs electricity to generate reducing equivalents needed to enzymatically fix CO_2 *in vivo* and synthesize an energy storage molecule like polyhydroxybutyrate (PHB) or a hydrocarbon fuel. In **Fig. 1B** CO_2 is first electrochemically reduced to a short-chain hydrocarbon like formate or formic acid *ex vivo* [27–29]. A microbe in the second cell absorbs electricity and further reduces and concatenates the initial fixation product to a longer-chain carbon compound. In both cases, electricity is absorbed into metabolism by either H_2-oxidation (H_2-mediated electromicrobial production; H_2-EMP) or EET (EET-mediated electromicrobial production; EET-EMP) **Fig. 1C**. A complete list of symbols used in this article is included in **Table S1**.

We define the electrical energy conversion efficiency as the rate of energy storage molecule production, $\dot{N}_{\text{fuel}}$, multiplied by the energy content per molecule, E_{fuel}, relative to the total electrical power input,

$$\eta_{\text{EF}} = \dot{N}_{\text{fuel}}\, E_{\text{fuel}} / P_{\text{e, total}}. \tag{1}$$

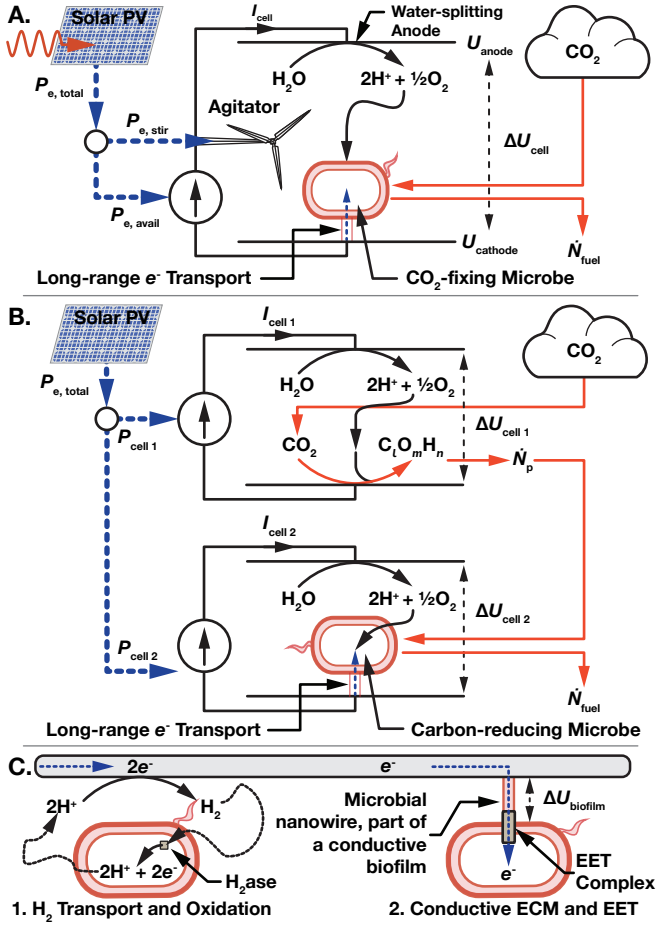

Figure 1: Overview of electromicrobial production technologies. (**A**) A microbe absorbs electrical power, $P_{\mathrm{e,\ avail}}$, through H_2-oxidation or through a conductive extracellular matrix (ECM) by extracellular electron transfer (EET) to power CO_2-fixation and biofuel production at a rate $\dot{N}_{\mathrm{fuel}}$. The total electrical power is used to drive a current, I_{cell}, across a whole-cell voltage, ΔU_{cell}, and can also be used to power an agitator. (**B**) The electrical power is split between two electrochemical cells. In the first CO_2 is reduced to a short chain hydrocarbon like formic acid at a rate $\dot{N}_{\mathrm{p}}$. The primary fixation product is then concatenated in the second cell by a H_2-oxidizing or electroactive microbe. (**C**) Electrons are transported to metabolism by either (1) diffusion or stirring of H_2 and oxidation by a hydrogenase (H_2ase) enzyme, or (2) across a conductive ECM and transport into an electroactive cell by a membrane-spanning EET complex. A bias voltage $\Delta U_{\mathrm{biofilm}}$ is required to drive current across the ECM.

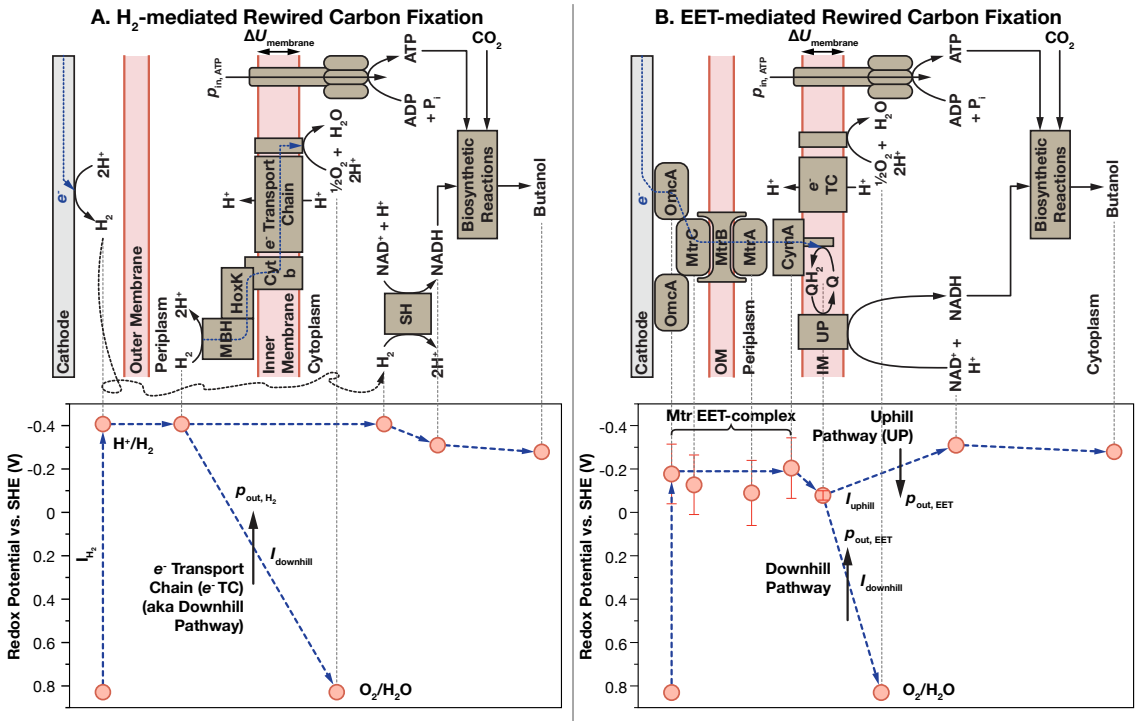

Figure 2: Energy landscapes for electromicrobial production. (**A**) In H_2-mediated electromicrobial production, the incoming H_2-current is used to directly reduce NAD(P)H or Ferredoxin (not shown), or is diverted into the conventional electron transport chain for ATP synthesis. For each electron sent downhill to reduce O_2 and H^+ to H_2O, $p_{\text{out, H}_2}$ are pumped across the inner membrane. To synthesize an ATP molecule, $p_{\text{in, ATP}}$ protons are released through the ATP synthase. (**B**) In Extracellular Electron Transfer (EET)-mediated electromicrobial production the incoming current is split between the uphill and downhill pathways. For each electron sent downhill, $p_{\text{out, EET}}$ protons are pumped across the inner membrane. Midpoint redox potentials for the Mtr EET complex components are from Firer-Sherwood *et al.* [26].

H_2-mediated Electromicrobial Production is Already Optimized but can be Improved by Swapping Out CO_2-fixation

Estimating the efficiency of *in vivo* CO_2-fixation (**Fig. 1A**) comes down to estimating $\dot{N}_{\text{fuel}}$ as a function of the electrical power available for electrochemistry, $P_{\text{e, avail}}$; the voltage across the electrochemical cell, ΔU_{cell}; and the number of electrons needed to generate the NAD(P)H, Ferredoxin (Fd), and ATP for synthesis of a single fuel molecule from CO_2, ν_{ef} (e = elementary charge) (**SI Text 1**),

$$\dot{N}_{\text{fuel}} \leq P_{\text{e, avail}} / \left(e \, \nu_{\text{ef}} \, \Delta U_{\text{cell}} \right) . \tag{2}$$

Therefore, the overall electrical to fuel efficiency for an *in vivo* CO_2-fixation scheme,

$$\eta_{\text{EF}} \leq E_{\text{fuel}} / \left(e \, \nu_{\text{ef}} \, \Delta U_{\text{cell}} \right) . \tag{3}$$

ν_{ef} can be estimated from molecular models of electron uptake. A schematic of the *Ralstonia eutropha* H_2-oxidation machinery (used by references [13, 14, 21]) is shown in **Fig. 2A**. The low

redox potential of H_2 (U_{H_2}) enables direct reduction of NADH by the cytosolic nickel-iron Soluble Hydrogenase (SH) (*R. eutropha* uses NADH rather than NADPH for CO_2-fixation) [30, 31]. While the *R. eutropha* genome does not code for any Fd-reducing di-iron hydrogenases, these could be readily added to it [32–34]. Thus, the microbe simply has to oxidize a number of H_2 molecules equal to the sum of NADH and Fd that it needs to synthesize a fuel molecule (the number of electrons needed is just double the number of H_2).

ATP is generated by injection of electrons from H_2-oxidation by the Membrane-Bound Hydrogenase (MBH) into the inner membrane electron transport chain [30, 31]; quantized energy transduction by proton pumping against the transmembrane voltage, $\Delta U_{\text{membrane}}$; reduction of a terminal electron acceptor at a redox potential U_{Acceptor}; and further quantized energy transduction by proton release through the ATP synthase and ATP regeneration.

Therefore, the number of electrons needed to synthesize a single fuel molecule through H_2-oxidation is (a full derivation is included in **SI Text 2**) ($\nu_{\text{f, NADH}}$, $\nu_{\text{f, Fd}}$, and $\nu_{\text{f, ATP}}$ are the number of NAD(P)H, Fd and ATP needed for synthesis of a single fuel molecule respectively),

$$\begin{aligned}\nu_{\text{ef, H}_2} = \\ &2\,\nu_{\text{f, NADH}} + 2\,\nu_{\text{f, Fd}} \\ &+ \nu_{\text{f, ATP}} \frac{\text{ceil}\left(\Delta G_{\text{ATP/ADP}} / e\,\Delta U_{\text{membrane}}\right)}{\text{floor}\left(\left(U_{H_2} - U_{\text{Acceptor}}\right)/\Delta U_{\text{membrane}}\right)}.\end{aligned} \tag{4}$$

These equations are numerically solved with the REWIREDCARBON package using estimates for the NAD(P)H, ATP and Fd requirements for isopropanol and 1-butanol synthesis (**Fig. S2**) from CO_2 fixed by the known natural CO_2-fixation cycles and the synthetic CETCH cycle [35] in **Table S2**.

The biggest source of uncertainty in the efficiency estimate is the transmembrane voltage ($\Delta U_{\text{membrane}}$). At the time of writing we are unaware of any direct measurement of $\Delta U_{\text{membrane}}$ in *R. eutropha* or the electroactive microbe *Shewanella oneidensis*. Therefore, in **Fig. 3** we present a range of efficiency estimates for $\Delta U_{\text{membrane}} = 80\,\text{mV}$ (BioNumber ID (BNID) 104082 [36]) to 270 mV (BNID 107135), with a central value of 140 mV (BNIDs 109774, 103386, 109775). Counterintuitively, the efficiency of H_2-mediated electromicrobial production trends downwards, moving from plateau to plateau, with increasing transmembrane voltage. (**Fig. S1A**). While the amount of energy stored per proton is lower at lower $\Delta U_{\text{membrane}}$, energy quantization losses are also reduced.

This framework estimates the electron requirement for isopropanol and butanol synthesis by the Bionic Leaf (H_2-EMP using the Calvin Cycle (CBB) for *in vivo* CO_2-fixation) to be $25^{+0.5}_{-3.5}$ and $31^{+0.5}_{-3.5}$ respectively. The maximum electricity to isopropanol conversion efficiency of the Bionic Leaf ($\Delta U_{\text{cell}} = 2\,\text{V}$ [14]) is estimated to be $41.6^{+0.8}_{-5.1}\%$ (**Bar C** in **Fig. 3**). This result just exceeds the maximum reported electrical to isopropanol efficiency of $39 \pm 2\%$ [14]. This match suggests that CO_2-fixation and biofuel synthesis in *R. eutropha* are already highly optimized.

How high could the efficiency go? Switching the product to butanol affords an improvement in H_2-EMP efficiency to $44.6^{+0.7}_{-4.5}\%$ and a significant improvement in ease of product recovery (**Bar**

D in **Fig. 3**). If the anode and cathode bias voltages could be reduced to zero, the efficiency of H_2-EMP electrical to 1-butanol efficiency could rise as high as $72.5^{+1.1}_{-7.4}\%$ (**Bar I**). However, given the already low cobalt phosphate electrode overpotentials [37] in the Bionic Leaf, raising the efficiency by this route might be impractical.

Could the efficiency of EMP be increased by altering just the biological part of the system? Following intuition, electrical to fuel efficiency increases with decreasing NAD(P)H, ATP and Fd requirements for CO_2 to biofuel conversion (**Fig. S3A-D**). The efficiencies of the six known naturally-occurring carbon fixation pathways and the synthetic CETCH pathway are shown in **Fig. 3**. The CETCH [35] cycle matches the efficiency of CBB (**Bar E**), while the naturally-occurring CO_2-fixation cycles 3HP-4HB (**Bar F**), rTCA (**Bar G**) and WL (**Bar H**) all perform better than the Calvin cycle, raising the electrical to fuel efficiency as high as $55.3^{+0.1}_{-1.1}\%$.

While the rTCA cycle and Wood-Ljungdahl pathway are both typically found in anaerobic and micro-aerophilic organisms, recent advances in compartmentalization in synthetic biology [38–40] could enable the implementation of these highly efficient pathways in synthetic organisms that operate under ambient atmospheric conditions and enable use of O_2 as a metabolic terminal electron acceptor.

H_2-mediated Electromicrobial Production Reaches Its Maximum Efficiency in Large Scale Systems

In principle, the efficiency of a electromicrobial production system could be independent of the specific activity of the carbon fixation pathway used (how many CO_2 molecules are fixed each second by each gram of enzyme). Fixing more CO_2 and storing more energy might simply require more cells operating in parallel. However, distributing electrical power through a H_2 mediator could pose energetic, geometric and safety challenges [31]. To assess these challenges, we built models of H_2-transport by diffusion and agitation.

The difficulty of H_2-transport is determined by the number and volume of cells needed to store the H_2-current, I_{H_2}, produced by the cell current (ξ_{eH_2} is the Faradaic efficiency of H_2 production, typically close to 1),

$$I_{H_2} = \xi_{eH_2}\, I_{\text{cell}}. \tag{5}$$

As hydrogenase enzymes are much faster than any carboxylating enzyme, the CO_2 fixation rate is the limiting factor in electron demand per cell. The rate of electron uptake by each cell depends on the number of electrons, ν_{ef}, and carbon atoms fixed, $\nu_{\text{Cf, fix}}$ (not just the number incorporated, ν_{Cf}), to synthesize each fuel molecule; and the rate and number of carbon-fixing enzymes, r_{fix} and ν_{fix} (**SI Text 3**),

$$\dot{\nu}_e = \nu_{\text{ef}}\, r_{\text{fix}}\, \nu_{\text{fix}}/\nu_{\text{Cf, fix}}. \tag{6}$$

Thus, the total number and volume of cells needed to store the H_2-current (n_{cells} is the cell density),

$$N_{\text{cells}} = I_{H_2}/e\,\dot{\nu}_e, \tag{7}$$

$$V_{\text{cells}} = N_{\text{cells}}/n_{\text{cells}}. \tag{8}$$

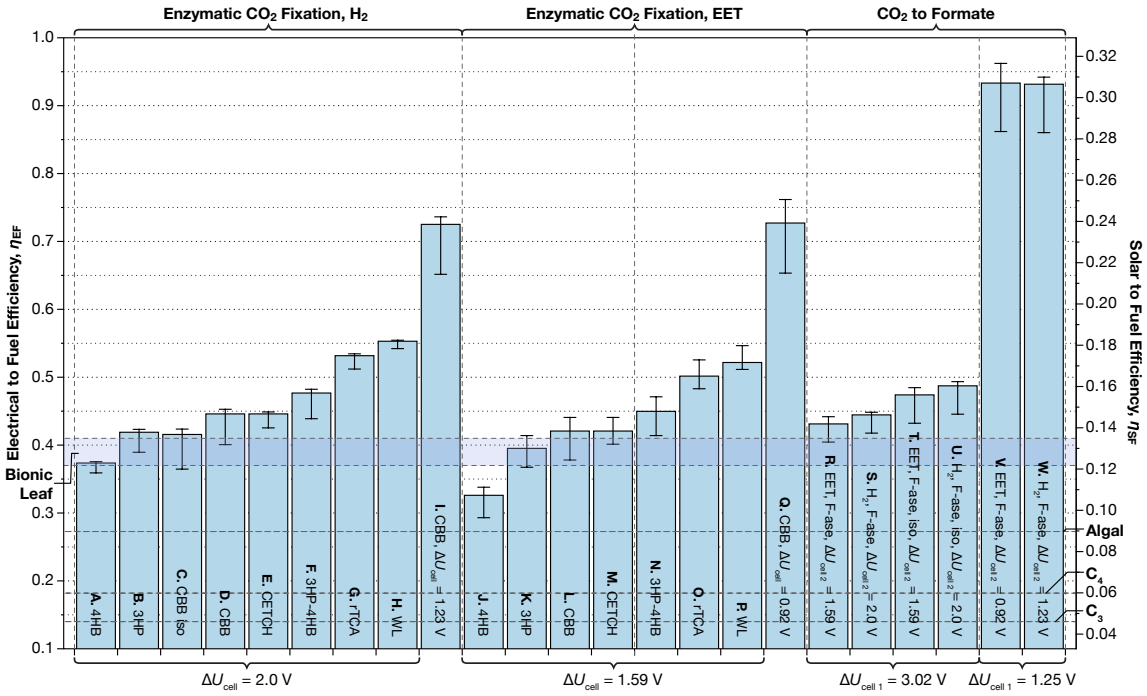

Figure 3: Projected lab-scale electrical and solar to biofuel efficiency of electromicrobial production schemes. The right axis is calculated by assuming a solar to electrical conversion efficiency of 32.9%, the maximum efficiency of a single junction Si solar PV [41]. Bars R to U assume a Faradaic efficency of CO_2 to formate reduction of 80%, while bars V and W assume 100% Faradaic efficiency. Whole cell voltages were calculated from the minimum redox potentials of H_2 and the Mtr EET complex [26] midpoint redox potentials, and from bias voltages reported by [13], [14], and [23]. Metabolic pathway data can be found in **Table S2**. All efficiences are for butanol production, except where noted as isopropanol (iso). This plot can be recreated with the `fig-co2fixation.py` program and `fig-co2fixation.csv` input file in the REWIREDCARBON package. 4HB = 4-hydroxybutyrate cycle; 3HP = 3-hydroxypropionate bicycle; CBB = Calvin-Benson-Bassham cycle; CETCH = (CoA)/ethylmalonyl-CoA/hydroxybutyryl-CoA; 3HP-4HB = 3-hydroxypropionate 4-hydroxybutyrate bicycle; rTCA = reductive tricarboxylic acid cycle; WL = Wood-Ljungdahl pathway.

H_2 could be transported by diffusion from the headspace of a reactor (where it is at a partial pressure P_{H_2}) without any additional energy input into the system (**Fig. 4A**). In order to achieve the high concentration gradient needed to drive rapid diffusion of H_2 (D_{H_2} and k_{H_2} are the diffusion and solubility coefficients for H_2 respectively), the cell culture has to be spread into a film with a height no greater than, and an area no less than (**SI Text 4**),

$$h_{\text{film}} \leq \sqrt{((2P_{H_2} D_{H_2} N_A)/ (k_{H_2} n_{\text{cells}} \dot{\nu_e}))}, \tag{9}$$

$$A_{\text{film}} \geq \frac{\xi_{eH_2} k_{H_2}^{1/2} P_{\text{e, avail}}}{e \Delta U_{\text{cell}} (2\dot{\nu_e} n_{\text{cells}} P_{H_2} D_{H_2} N_A)^{1/2}}. \tag{10}$$

The area of a electromicrobial production system supplied by H_2-diffusion scales linearly with input power while the film thickness remains the same. *R. eutropha* is typically grown under an atmosphere containing H_2, O_2 and CO_2 at a ratio of 8:1:1 [42]. At the laboratory-scale, the H_2 partial pressure is usually restricted to 5% of a total pressure of 1 atmosphere in order to reduce the risks of H_2 explosion [42]. If supplied by a solar photovoltaic (PV), the area of the film rela-

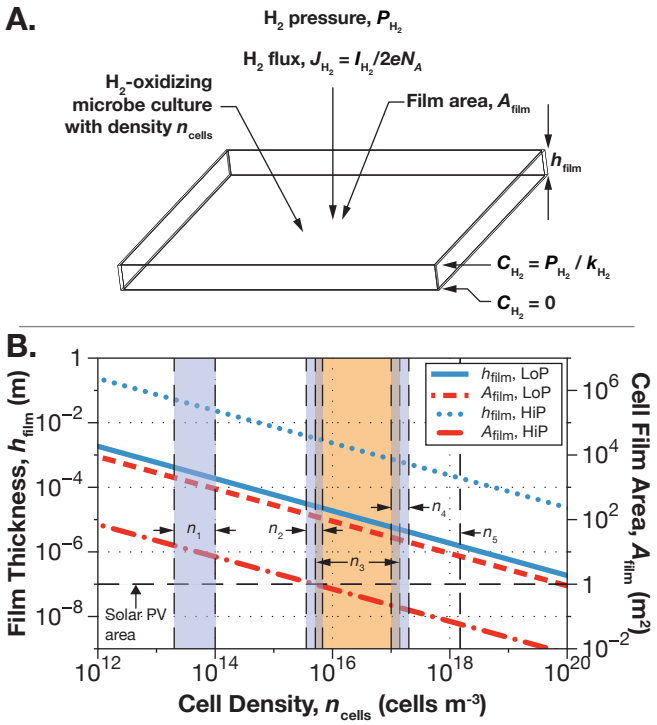

Figure 4: H_2-transport by diffusion to enable scale up of H_2-mediated electromicrobial production systems using the Calvin cycle (CBB) to convert CO_2 to butanol. (**A**) Geometry for H_2 mixing by diffusion. (**B**) Maximum height of cell culture that can be supplied with H_2 by diffusion and corresponding area of culture needed to convert 330 W of electrical power (produced by a perfectly efficient $1\,m^2$ single-junction Si solar PV illuminated by $1,000$ W of solar power) at H_2 partial pressures of 5066 Pa (5% of atmospheric pressure; LoP) and 81 MPa (80% of $1000\times$ atmospheric pressure; HiP). Five important cell density regimes are noted in panel **B**: n_1: laboratory grown cultures of *E. coli* in exponential phase; n_2: cyanobacteria grown to maximum density; n_3: cultures of *E. coli* at saturating density; n_4: H_2-oxidizing microbes grown to maximum density; and n_5: and saturating cultures of industrially-grown yeast (**SI Text 5**) and **Table S5**. Panel **B** can be recreated with the `fig-h2diffusion.py` programs and corresponding input file in the REWIREDCARBON package. To ease interpretation of panel **B** we have re-drawn this panel as two separate panels, each with a single curve representing the area and thickness of the cell culture film at each pressure in **Fig. S6**.

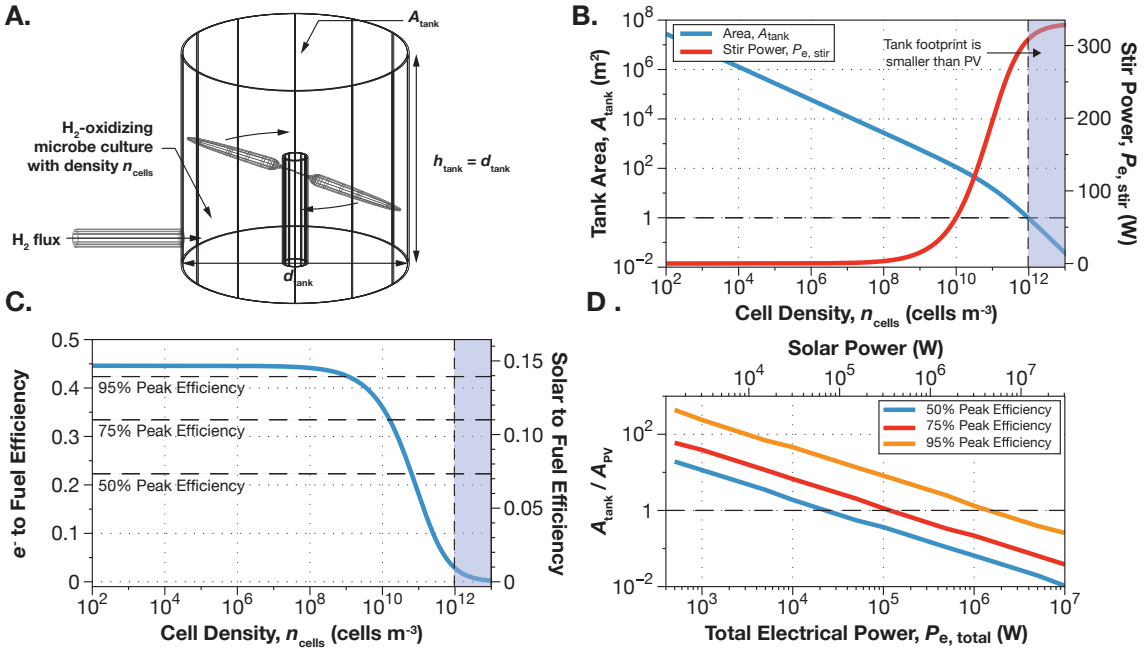

Figure 5: Scale up of H_2-mediated electromicrobial production systems using the Calvin cycle (CBB) to convert CO_2 to 1-butanol. (**A**) Geometry for mixing H_2 by agitation. (**B**) As cell density is increased to reduce system footprint, the power required to mix H_2 by agitation increases, eventually consuming all of the 330 W available to the system, (**C**) reducing the electricity to fuel efficiency to zero. (**D**) But, the system fooprint to PV area ratio at which the system achieves 50, 75 and 95% of its peak efficiency falls with increasing input power to the system (and solar PV area). Panels **B** to **D** in this plot can be recreated with the `fig-h2agitation-B` to `D.py` programs and the corresponding input files in the REWIREDCARBON package. Note that the cell densities shown here are much lower than those highlighted in **Fig. 4**.

tive to the solar PV area, A_{PV}, will remain constant. A plot of film thickness and area versus cell culture density is shown for two systems supplied by a $1\,m^2$ solar PV in **Fig. 4B**: the first with a headspace H_2 partial pressure of 5,066 pascals (Pa) (5% of 1 atmosphere; O_2 and CO_2 will both be at a partial pressure of 633.25 Pa and the system will be balanced with N_2), and the second with a H_2 partial pressure of 81×10^6Pa (80% of 1,000 atmospheres; O_2 and CO_2 will both be at a partial pressure of 10.1×10^6Pa).

For the ambient pressure system, the film area (and potential footprint of the system) is greater than the area of the PV supplying it for even the highest cell densities seen in bio-industrial applications. At the highest reported autotrophic density for *R. eutropha* (density region **4**; n_4 [43]), the film area is between 20 and $28\,m^2$. The large film area requirement for H_2-transport by diffusion at ambient pressures may not be insurmountable. Bioreactors with high internal areas but relatively small footprints could be constructed by stacking planar cell layers on top of one another, or using hollow fibers in which cells are immobilized on the walls of the fiber and reactant gases are flowed along its inner and outer surfaces [44].

Furthermore, by increasing the H_2 partial pressure to 81×10^6Pa, the cell film area can be reduced to $1\,m^2$ by a density of $\approx 5 \times 10^{15}$ cells m^{-3}, inside the range of typical cyanobacterial cell

densities (density region **2**; n_2).

H_2-diffusion systems could enable very high efficiency, but may come at the cost of high initial expenditure, complexity, maintenance, potential for H_2 escape, and difficulty in removing product.

Intuitively, agitation allows H_2-transport without the need for extreme system geometries, high pressures or both, at the expense of power input. The input power to the electrochemical cell is the total available electrical power, $P_{\text{e, total}}$, minus any power needed to agitate the system,

$$P_{\text{e, avail}} = P_{\text{e, total}} - P_{\text{e, stir}}. \tag{11}$$

We considered a cylindrical stirred tank of cells that continuously distributes H_2 supplied by a sub-surface pipe (**Fig. 5A**). We numerically solved a set of coupled equations linking H_2 production, consumption, gas transfer rate, cell culture volume, and the power required for gas mixing through an iterative algorithm in the REWIREDCARBON package using a formalism compiled by Van't Riet [45] until a self consistent set of solutions were found (**SI Text 6**). The solution to these equations for a system supplied with 330W of electrical power from a $1\,\text{m}^2$ solar PV are plotted in **Figs. 5B** to **5D**.

At low cell densities and high system footprints (and hence volumes), the power required to transport H_2 is low, while at low volumes the effort to stir is much greater (**Fig. 5B**). Intuitively, anyone who has grown cell culture understands that it is much easier to agitate a large cell culture (*e.g.* a 1 L flask) than a smaller culture (*e.g.* a $200\,\mu$L well in a 384-well plate). This creates a conundrum, $P_{\text{e, stir}}$ can be minimized, but at the expense of a tank footprint much larger A_{PV}. Or, the tank footprint can be reduced to less than A_{PV}, but at the expense of diverting more and more solar power to mixing H_2 (**Fig. 5B**). This means that the efficiency of the electromicrobial production system (**Fig. 5C**) drops precipitously from its maximum potential value to almost zero as the footprint of the system is reduced to allow it to fit under the solar PV supplying it.

The footprint-efficiency dilemma can be resolved by operating at higher input power. We calculated the system footprint to PV area ratio ($A_{\text{tank}}/A_{\text{PV}}$) at which the system achieves 50%, 75%, and 95% of its maximum potential efficiency in **Fig. 5D**. For small scale systems (500 to 10^4 W of solar power) footprints of 60× to 7× the area of the solar PV supplying them are required to achieve 75% of maximum efficiency. However, for large scales systems exceeding 1.1×10^5 W of electrical power, the system footprint begins to shrink below that of the solar PV supplying it. Systems supplied by more than 1.1×10^6 W of electrical power can achieve 95% of maximum efficiency and still have a footprint smaller than the solar PV supplying them.

EET Matches the Efficiency of H_2 and can Achieve High Efficiencies at Small Scales

Extracellular electron transfer (EET) could allow scale up of electromicrobial production through the use of a conductive biofilm to supply electrons to the cell (**Fig. 1C**). Electroactive microbes can transfer charge to, from and between external substrates like metals and even electrodes at

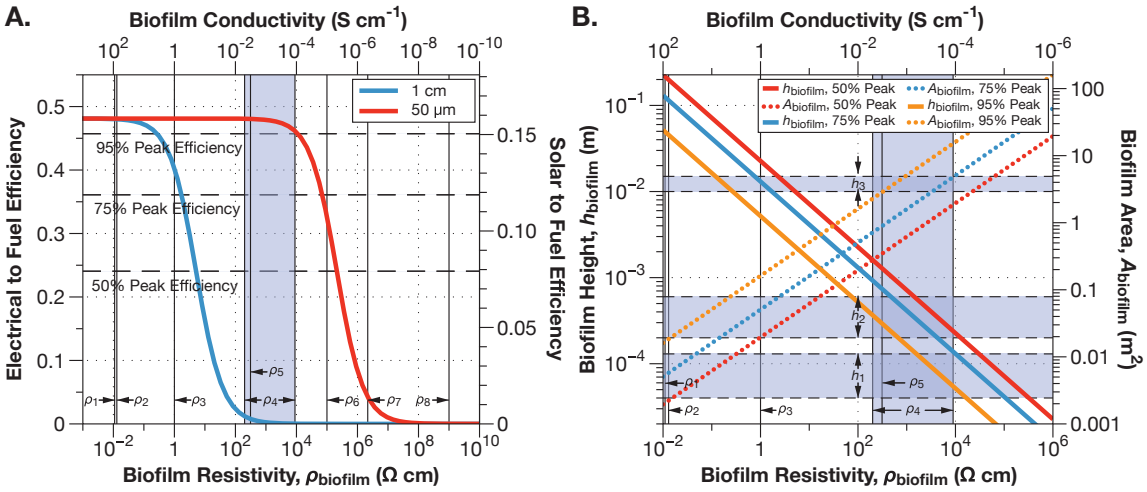

Figure 6: Biofilm resistivity determines efficiency losses in the scale-up of EET-mediated electromicrobial production. The system shown here has an anode bias voltage of 0.47 V, fixes CO_2 with the Calvin cycle and produces butanol (**A**) The electrical to fuel efficiency of a electromicrobial production system drops after a threshold resistivity is reached. The thicker the biofilm, the earlier this drop occurs. (**B**) Maximum biofilm thickness and minimum area needed to achieve 50, 75 and 95% of peak efficiency. This plot can be recreated with the `fig-EETscaleup- A.py` and `B.py` programs and corresponding input files in the REWIREDCARBON package. Representative conductive matrix resistivities and heights: ρ_1: high conductivity polypyrrole; ρ_2: individual cable bacteria filaments; ρ_3: individual *S. oneidensis* nanowires; ρ_4: bulk *G. sulfurreducens* and *S. oneidensis* biofilm resistivities; ρ_5: polypyrrole conductive matrix for *S. oneidensis*; ρ_6: bulk *E. coli* biofilm; ρ_7: HBr doped polyaniline; ρ_8: low conductivity polypyrrole; h_1: *G. sulfurreducens* biofilms; h_2: polypyrrole conductive matrix for *S. oneidensis*; h_3: cable bacteria biofilms and individual filaments (**SI Text 9**) and **Tables S3** and **S4**). To ease interpretation of panel **B** we have re-drawn this panel as three separate panels, each with a single curve representing the area and thickness of the biofilm at each efficiency in **Fig. S7**.

distances up to a centimeter from the cell surface and use specialized metalloprotein complexes that connect the cell surface to the electron transport chain in the inner membrane (**Fig. 2B**) [46–49].

The energy landscape of EET has raised concerns about its use in electromicrobial production. The redox potentials of the membrane spanning cytochrome complex (Mtr in *S. oneidensis* at ≈ -0.1 V vs. the Standard Hydrogen Electrode (SHE) [50]) and the inner membrane electron carriers menaquinone (-0.0885 V [50]) and ubiquinone (0.1 V [50]) are too high to directly reduce NAD^+ to NADH (-0.32 V [51]).

Nature suggests that the redox potential mismatch between the inner membrane and NAD^+ is not insurmountable. Today, electroactive iron-oxidizing microbes are able to draw electrons from the oxidation of iron minerals at redox potentials from +0.7 to $\approx$ 0.1 V to power CO_2-fixation and autotrophic metabolism [52, 53]. In the distant past it is thought that iron-oxidation powered the global carbon cycle [54]. It is speculated that an "uphill pathway" is able to lower the redox potential of electrons in the quinone pool to that of NAD^+ [50].

Recently Rowe *et al.* [55] provided compelling evidence that a reverse electron transport chain providing an uphill pathway operates in *S. oneidensis*. While the the full complement of genes encoding this pathway remains unknown (although some parts have been found [55–58]), this

pathway is proposed to operate by directing part of a cathodic current downhill in energy to a terminal electron acceptor and pumping protons across the inner membrane. The energy stored in the proton gradient is used to power NAD^+ reduction and ATP production. A model for electron uptake by EET is shown in **Fig. 2B**.

Due to the need to sacrifice some current to generate a proton gradient for NAD^+ (and possibly Fd) reduction, the number of electrons needed to produce the NADH, Fd and ATP for synthesis of a single fuel molecule through EET is higher than in H_2-oxidation (a full derivation is included in **SI Text 7**),

$$\begin{aligned}
&\nu_{\text{ef, EET}} = \\
&2\,\nu_{\text{f, NADH}} + 2\,\nu_{\text{f, Fd}} \\
&+ \nu_{\text{f, ATP}}\,\frac{\text{ceil}\left(\Delta G_{\text{ATP/ADP}}/e\,\Delta U_{\text{membrane}}\right)}{\text{floor}\left(\left(U_{\text{Q}} - U_{\text{Acceptor}}\right)/\Delta U_{\text{membrane}}\right)} \\
&+ 2\,\nu_{\text{f, NADH}}\,\frac{\text{ceil}\left(U_{\text{NADH}} - U_{\text{Q}}/\Delta U_{\text{membrane}}\right)}{\text{floor}\left(\left(U_{\text{Q}} - U_{\text{Acceptor}}\right)/\Delta U_{\text{membrane}}\right)} \\
&+ 2\,\nu_{\text{f, Fd}}\,\frac{\text{ceil}\left(U_{\text{Fd}} - U_{\text{Q}}/\Delta U_{\text{membrane}}\right)}{\text{floor}\left(\left(U_{\text{Q}} - U_{\text{Acceptor}}\right)/\Delta U_{\text{membrane}}\right)}.
\end{aligned} \tag{12}$$

However, counterintuitively, EET-mediated electromicrobial production is not dramatically less efficient than H_2-mediated electromicrobial production (**Fig. 3**). While the number of electrons needed to produce a molecule of fuel is higher, the whole-cell voltage in an EET-mediated system is lower than in a H_2-mediated system ($\Delta U_{\text{cell}} \geq 1.23\,\text{V}$ for H_2 but only $\geq 0.92\,\text{V}$ for EET) as the redox potential of Mtr is much lower than H_2 [26]. Furthermore, the bias voltages at lab-scale remain approximately the same [7], meaning more total current is available to an EET-mediated system. However, EET-mediated electromicrobial production is approximately twice as sensitive to changes in transmembrane voltage than a H_2-mediated system (**Fig. S1**).

The scale up of EET-mediated electromicrobial production is potentially much easier than H_2-EMP. We built a model of scale up for an EET-mediated system assuming that the dominant source of overpotential is the resistivity of the biofilm. We assumed that the biofilm could be modeled as an Ohmic resistor, so that the bias voltage needed to transport electrons across it is,

$$\Delta U_{\text{biofilm}} = \rho_{\text{biofilm}}\,h_{\text{biofilm}}\,I_{\text{cell}}/A_{\text{biofilm}}. \tag{13}$$

We developed a set of five coupled equations to solve for the cell current I_{cell}, the bias voltage needed to drive current across the biofilm $\Delta U_{\text{biofilm}}$, the area of the biofilm A_{biofilm}, the total number of cells in the biofilm N_{cells}, and the volume of the biofilm V_{biofilm} in **SI Text 8**. These equations were solved numerically and the results shown in **Fig. 6**. Unlike agitation based systems, the energy cost of electron transport by EET scales linearly with system size: for a given biofilm resistivity, the ratio of the areas of the biofilm and the solar panel supplying it with electricity remains constant. Moreover, there is no obvious penalty for operating small-scale systems as there is with agitation.

At low resistivities (high conductivities) the biofilm overpotential is small, allowing a conductive matrix system to achieve close to its maximum possible efficiency, set only by the thermodynamic

minimum voltages and any non-biofilm bias in the system (**Fig. 6A**). However, above a critical resistivity, the efficiency drops precipitously. For a 50 μm thick film, the efficiency starts to drop below 95% of maximum at a resistivity of $\approx 10^5\,\Omega\,\text{cm}$, considerably higher than the commonly reported resistivities of *Geobacter sulfurreducens* and *S. oneidensis* biofilms (ρ_4 in **Fig. 6A**, **SI Text 9**) [59–61]. Note that the peak efficiency shown in **Fig. 6A** exceeds that shown in **Fig. 3** Bar L as we assume only anode bias.

As the resistivity of the conductive matrix increases, its thickness must decrease and its area increase in order to maintain a given efficiency. In contrast to a 50 μm film, a 1 cm thick film suffers a drop in efficiency to 50% of maximum at a resistivity of only $\approx 10\,\Omega\,\text{cm}$, well below the resistivity range of *G. sulfurreducens* and *S. oneidensis* biofilms [59–61], but above the reported resistivities of individual *S. oneidensis* nanowires (ρ_3 in **Fig. 6A**) [62] and individual filaments produced by the cable bacterium *Thiofilum facile* (ρ_2 in **Fig. 6A**) [63].

Fig. 6B shows the maximum conductive matrix thickness and minimum area able to achieve a given fraction of peak efficiency as a function of resistivity. If 50% of peak efficiency is acceptable, then the biofilm area can be constrained to $1\,\text{m}^2$ (equal to that of the solar PV supplying it) if the biofilm resistivity is $2,650\,\Omega\,\text{cm}$, well within the range of *G. sulfurreducens* and *S. oneidensis* biofilm resistivities. However, the corresponding film thickness is 440 μm, about 3$\times$ the height of most commonly observed *G. sulfurreducens* and *S. oneidensis* biofilms (although Renslow *et al.* did observe *S. oneidensis* films as thick as 450 μm). However, artificial polypyrrole conductive ECMs have been produced that are as thick as 600 μm, and have resistivities as low as $312\,\Omega\,\text{cm}$ (ρ_5 in **Fig. 6**). Were the film area increased to $3.4\,\text{m}^2$, the film thickness could be reduced to 130 μm, within the range of commonly observed *G. sulfurreducens* and *S. oneidensis* biofilm thicknesses. The biofilm resistivity would only need to be $29,000\,\Omega\,\text{cm}$, above that of many conductive biofilms, perhaps allowing some conductivity to be sacrificed to enable increased CO_2 inflow or biofuel outflow.

On the other hand, if a thickness of 130 μm and resistivity of $1,600\,\Omega\,\text{cm}$ are simultaneously achievable, 95% of peak efficiency can be achieved if a $6.4\,\text{m}^2$ biofilm area is acceptable. If a $1\,\text{m}^2$ biofilm with a resistivity $38\,\Omega\,\text{cm}$ and a thickness of 830 μm could be produced, 95% of peak efficiency could be achieved.

If a biofilm could be produced with a 1 cm thickness (within the range of biofilm thickness produced by cable bacteria; h_3 in **Fig. 6**), a resistivity of $5\,\Omega\,\text{cm}$ (above the resistivity of individual *S. oneidensis* nanowires, and well above that of individual *T. facile* filaments, but below that of the minimum resistivity calculated by Polizzi *et al.* of $30\,\Omega\,\text{cm}$ [64]), and an area of only $0.044\,\text{m}^2$ then 50% of maximum efficiency could be achieved. If a biofilm of 1 cm thickness, with a resistivity of $0.26\,\Omega\,\text{cm}$, and an area of $0.079\,\text{m}^2$, 95% of peak efficiency could be achieved.

Finally, if 95% of peak efficiency were desired, but only a thin biofilm of 55 μm with a high resistivity of $8,952\,\Omega\,\text{cm}$ could be produced, then an area of $15\,\text{m}^2$ would be required.

Electrochemical CO_2 Fixation Could Allow Very High Electricity to Fuel Conversion Efficiencies

H_2-oxidation and EET could be an important complement to electrochemical CO_2-fixation technologies. Current electrochemical CO_2-fixation systems typically produce compounds with no more than two carbons that are often not completely reduced [27]. By contrast, most drop-in fuels require at least 2 to 3 carbons, with 8 electrons each.

Li *et al.* demonstrated the reduction of formate to isobutanol and 3-methyl-1-butanol (3MB) by the H_2-oxidizing microbe *R. eutropha* [21]. While this work relied upon oxidation of formate to CO_2 and subsequent re-fixation by RuBisCO, recent advances in artificial computational metabolic pathway could enable enzymatic transformation without reliance upon this bottleneck [65, 66].

The efficiency of electrochemical CO_2-fixation electromicrobial production schemes is set by the number of electrons $\nu_{\mathrm{e,\ add}}$ needed to produce the NAD(P)H, Fd and ATP needed to transform the primary fixation product to a biofuel; the charge needed to synthesize the primary electrochemical CO_2-fixation product, $e\,\nu_{\mathrm{ep}}$; the number of carbons in each primary fixation product, ν_{Cp}; the Faradaic efficiency of the first electrochemical reaction, ξ_{I1}, (while we are calculating an upper limit on efficiency we have rarely seen $\xi_{\mathrm{I1}} > 0.8$ [27]); the efficiency of carbon transfer to the second cell ξ_{C}; and the Faradaic efficiency in the second cell ξ_{I2} (**SI Text 10**),

$$\eta = \frac{P_{\mathrm{e,\ avail}}\, E_{\mathrm{fuel}}\, \xi_{\mathrm{I2}}}{e\,\nu_{\mathrm{e,\ add}} \left(\Delta U_{\mathrm{cell\ 1}} \left(\frac{\nu_{\mathrm{P}}\, \nu_{\mathrm{ep}}\, \nu_{\mathrm{Cp}}\, \xi_{\mathrm{I2}}}{\xi_{\mathrm{I1}}\, \xi_{\mathrm{C}}\, \nu_{\mathrm{e,\ add}}} \right) + \Delta U_{\mathrm{cell\ 2}} \right) P_{\mathrm{input,\ total}}}. \tag{14}$$

Even with only 80% Faradaic efficiency for the conversion of CO_2 to formate, the electrical energy to butanol conversion efficiency of the formolase artificial metabolic pathway [65] powered by either H_2-oxidation or EET exceeds all fully enzymatic CO_2-fixation pathways with the exception of the rTCA cycle and Wood-Ljungdahl pathway **Fig. 3**, and suffers no complications of O_2-sensitivity.

Conclusions

What combination of electron uptake, electron transport, and carbon fixation is the best for electromicrobial production? The model of electromicrobial production lets us sketch out a roadmap for how to proceed with the technology. We outline 10 possible development and deployment scenarios that could be pursued in the near and further future in **Table 1** along with their advantages, disadvantages, and suggested niche.

This work shows that H_2-EMP using the Calvin cycle [13, 14], is already highly optimized. This means that engineering the host microbe (*e.g. R. eutropha*) by adjusting expression levels of enzymes already encoded in the genome or changing the transmembrane voltage are unlikely to produce gains of more than a few percentage points in electricity to biofuel conversion efficiency.

#	**Scenario**	**Advantages**	**Drawbacks**	**Display Item**
1	Metabolically engineer *R. eutropha* by adjusting enzyme expression.	Straightforward genetic engineering.	Unlikely to produce significant gains in electricity to biofuel conversion efficiency.	Fig. 3 Bars C and D.
2	Engineer H_2-oxidizing chassis with more efficient CO_2 fixation	Significant increase in electrical to biofuel conversion efficiency.	Significant increase in genetic engineering complexity. O_2-sensitivity (rTCA and WL).	Fig. 3 Bars E, F, G, and H
3	Engineer H_2-oxidizing chassis with formate assimilation pathway.	Significant increase in electrical to biofuel conversion efficiency Less complex genetic engineering. No known O_2-sensitivity issues.	Increased system complexity due to electrochemical CO_2 reduction.	Fig. 3 Bars S and U
4	Deploy H_2-EMP in large volume stirred tank reactor at ambient pressure.	Small footprint. Low system complexity.	Potential for H_2 escape and energy loss. Only efficient at large scales ($\geq 1\,MW$)	Fig. 5
5	Deploy H_2-EMP in a diffusional hollow fiber reactor at ambient pressure.	Efficient at all power scales.	High complexity due to large internal surface area. Potential for H_2 escape and energy loss.	Fig. 4B
6	Deploy H_2-EMP in a diffusional hollow fiber reactor at high pressure.	Efficient at all power scales. Significantly reduced internal area compared to ambient pressure case.	Increased complexity due to need to maintain high internal gas pressure. Explosive atmosphere. Potential for H_2 escape and energy loss.	Fig. 4B
7	Engineer EET chassis with CO_2-fixation pathway.	No volatile intermediate (H_2).	Small efficiency loss compared with H_2-oxidizing chassis organism. Highly complex genetic engineering.	Fig. 3 Bars L, M, N, O, and P
8	Engineer EET chassis with a formate assimilation pathway.	Potential significant increase in electrical to biofuel conversion efficiency over a chassis using the CBB cycle. Less complex genetic engineering. No known O_2-sensitivity issues.	Increased system complexity due to electrochemical CO_2 reduction.	Fig. 3 Bars R and T
9	Deploy EET-EMP with a conductive extracellular matrix (ECM).	No volatile intermediate (H_2) Potential for low internal area reactor Room for reduction in ECM conductivity to allow CO_2 access and product extraction	Small efficiency loss relative to H_2-transport Potential difficulty in cultivating and maintaining large area ECMs. Product extraction and CO_2 access to the biofilm could compromise conductivity. Engineering biofilm formation poses significant genetic engineering challenge.	Fig. 6
10	Engineering a quantum dot-EET-EMP hybrid.	No volatile intermediate (H_2). Potential for extremely low complexity system.	High complexity of genetic engineering to introduce CO_2-fixation of any sort to EET-chassis organism.	

Table 1: Future research and development, and deployment scenarios for electromicrobial production. ECM = Extra-Cellular Matrix.

One genetic engineering route to increased electrical to biofuel conversion efficiency (from $\approx 40\%$ to as high as 55% at lab scales) is replacement of the familiar Calvin cycle with any one of the CETCH, 3HP-4HB, rTCA or WL CO_2-fixation pathways. This is approach is not for the faint hearted. However, recent impressive progress in engineered the Calvin cycle into *E. coli* makes this a tantalizing possibility [67, 68]. Furthermore, the need to use O_2 as a terminal electron acceptor to achieve maximum efficiency means that the O_2-sensitivity of the rTCA and WL pathways will need to be mitigated by developing O_2-tolerant versions of currently O_2-sensitive enzymes in these pathways, or sequestering these enzymes inside O_2-impermeable compartments inside the cell.

An alternative route to significantly enhanced efficiency is dispense with *in vivo* CO_2-fixation and replace it with *ex vivo* electrochemical CO_2 reduction and *in vivo* formate assimilation. This approach is much more genetically tractable and achieves efficiency gains comparable to replacing the Calvin cycle wih the rTCA cycle. Additionally, there is room for further improvement as new artificial pathways for processing electrochemically fixed CO_2 are invented. However, this approach adds further system complexity and potential cost.

The optimization of H_2-EMP with the Calvin cycle raises the question: is it time to take it out of the lab? Agitation is the most mature, lowest cost, and most easily implemented technology for electron transport considered in this article. However, the high energy cost of stirring small volumes means that the smallest increment of storage that can be built is $\approx 1\,\mathrm{MW}$, about the size of a large solar farm. This is very large relative to residential storage needs (the average American home uses electrical energy at the rate of about $1.3\,\mathrm{kW}$), but tiny compared to the production needs for aviation fuel (when converted to jet fuel with $\approx$ 50% efficiency $1\,\mathrm{MW}$ corresponds to $\approx 50\,\mathrm{L\,hr^{-1}}$. A 787-9 consumes fuel at the rate of $\approx 7,000\,\mathrm{Lhr^{-1}}$).

Its not clear that H_2-EMP will ever take on batteries for home energy storage. H_2-EMP could operate very efficiently at a small power scale if H_2 is transported by diffusion. However, this approach demands a high internal area reactor. This problem can be ameliorated by operating at high H_2 pressure, but it is likely that this will increase cost, and incur significant safety risks. We would be foolish if we dismissed this approach outright, but we believe this analysis highlights significant technology risks.

Counter to intuition, the efficiency of EET-EMP using a reverse electron transport chain could almost match that H_2-mediated electromicrobial production with laboratory overpotentials. Additionally its possible to grow conductive ECMs with sufficiently high conductivities and thicknesses that a high-efficiency, low-footprint, low internal area system could be produced with the microbes we already have available today. In principle, EET-EMP coupled to a self-assembled conductive extracellular matrix (ECM) could reduce construction costs; allow us to dispense with volatile intermediates like H_2, reducing safety concerns; and allow operation in an ambient atmosphere, potentially dramatically reducing operating costs as well. Furthermore, there is no obvious penalty for operating small-scale systems, meaning that EET-EMP could enable highly distributed energy storage. However, as of today there is no easily genetically-engineered microbe capable of both electron uptake by EET and CO_2 fixation, meaning that this would need to be created. It is unclear if the reductions in cost and system complexity are worth the trade-off in the amount of complex microbe engineering that would be needed for such a feat. As of today,

we are unaware of the full complement of genes needed for the reverse electron transport chain. Furthermore, it is unclear how easy it would be for self-assembly of the large area ECMs that this approach would rely upon. For ECMs with conductivities similar to those produced by *G. sulfurreducens* and *S. oneidensis* several square meters of ECM would be required for every square meter of solar panel. In the lab, ECMs with areas exceeding only a few square centimeters are rarely seen [69]. If the very high reported conductivities of cable bacteria ECMs can be reproduced, these could reduce the ECM area to only a few square centimeters. Recent developments in the construction of engineered biofilms [70] suggests that it might be possible to build a biologically synthesized conductive matrix that is tailored for electrosynthesis with low resistivity, high thickness, high area, and high accessibility for CO_2 and product egress.

Recent developments in coupling photo-chemistry with EET [71] opens up the possibility of constructing quantum-dot (QD)-microbe hybrids that directly inject electrons in to the EET complex and then into metabolism. This would allow for the development of a system free of photovoltaics and electrodes that could be deployed at potentially extremely low cost. The possibility of adjusting the redox potential of the Mtr EET complex without significantly reducing efficiency (**Fig. S5**), along with the tunability of the electronic structure of quantum dots could allow significant room for engineering. Here, the potential for significant cost reduction could make for a significant payoff for the complex genetic engineering required to combine EET and carbon fixation.

The upper limits of efficiency of the EMP schemes presented here exceed those of all known forms of photosynthesis. Are these gains in efficiency worth pursuing? Can EMP achieve a significantly higher fraction of its theoretical efficiency in the real world than photosynthesis at an affordable cost? We cannot guarantee this, but the framework developed here gives us and other investigators the ability to rapidly understand the potential bang for buck of EMP schemes (of which there are many more than presented here). We hope that with the roadmap this framework gives, we and others in parallel can rapidly advance the field in multiple directions.

Materials and Methods

The theory presented in this work was implemented in the RewiredCarbon suite of software developed with Python with the SciPy [72] and NumPy [73] libraries. Initial visualization was implemented with Matplotlib [74]. All computer code is available at github.com/barstowlab/rewiredcarbon

Acknowledgment

This work was supported by a Career Award at the Scientific Interface from the Burroughs-Wellcome Fund (to B.B.), Princeton University startup funds (B.B.), Cornell University startup funds (B.B.), a Cornell Energy Systems Institute (CESI) Postdoctoral Fellowship (A.M.S) and by U.S. Department of Energy Biological and Environmental Research grant DE-SC0020179 (B.B.)

References

[1] Huhne, C., Jones, C., Foster, A. & Ewing, F. UK Renewable Energy Roadmap. Tech. Rep. (2011). URL https://assets.publishing.service.gov.uk/government/uploads/system/uploads/attachment-data/file/48128/2167-uk-renewable-energy-roadmap.pdf.

[2] Schmalensee, R. The Future of Solar Energy: an Interdisciplinary MIT Study. Tech. Rep. (2015). URL http://energy.mit.edu/research/future-solar-energy/.

[3] Annual Energy Outlook 2019 with Projections to 2050. Tech. Rep. (2019). URL https://eia.gov/aeo.

[4] Frew, B. A., Becker, S., Dvorak, M. J., Andresen, G. B. & Jacobson, M. Z. Flexibility mechanisms and pathways to a highly renewable US electricity future. *Energy* **101**, 65–78 (2016).

[5] Shaner, M. R., Davis, S. J., Lewis, N. S. & Caldeira, K. Geophysical constraints on the reliability of solar and wind power in the United States. *Energy & Environmental Science* **11**, 914–925 (2018).

[6] Cebulla, F., Haas, J., Eichman, J., Nowak, W. & Mancarella, P. How much electrical energy storage do we need? A synthesis for the U.S., Europe, and Germany. *Journal of Cleaner Production* (2018).

[7] Salimijazi, F., Parra, E. & Barstow, B. Electrical Energy Storage with Engineered Biological Systems. *Journal of Biological Engineering* **13**, 1–21 (2019). URL https://jbioleng.biomedcentral.com/articles/10.1186/s13036-019-0162-7.

[8] Herzog, H. J. *Carbon Capture* (MIT Press, 2018).

[9] Committee on Developing a Research Agenda for Carbon Dioxide Removal and Reliable Sequestration. Negative Emissions Technologies and Reliable Sequestration: A Research Agenda. Tech. Rep. (2019).

[10] Rabaey, K. & Rozendal, R. A. Microbial electrosynthesis - Revisiting the electrical route for microbial production. *Nature Reviews Microbiology* **8**, 706–716 (2010). URL http://dx.doi.org/10.1038/nrmicro2422.

[11] Rabaey, K., Girguis, P. & Nielsen, L. K. Metabolic and practical considerations on microbial electrosynthesis. *Current Opinion in Biotechnology* **22**, 371–377 (2011). URL http://dx.doi.org/10.1016/j.copbio.2011.01.010.

[12] Lips, D., Schuurmans, J. M., Branco Dos Santos, F. & Hellingwerf, K. J. Many ways towards 'solar fuel': Quantitative analysis of the most promising strategies and the main challenges during scale-up. *Energy and Environmental Science* **11**, 10–22 (2018). URL http://dx.doi.org/10.1039/C7EE02212C.

[13] Torella, J. P. *et al.* Efficient solar-to-fuels production from a hybrid microbial-water-splitting catalyst system. *Proceedings of the National Academy of Sciences* **112**, 2337–2342 (2015). URL http://www.pnas.org/lookup/doi/10.1073/pnas.1503606112.

[14] Liu, C., Colón, B., Ziesack, M., Silver, P. & Nocera, D. Water splitting biosynthetic system with CO_2 reduction efficiencies exceeding photosynthesis. *Science* **352**, 1210–1213 (2016). URL `https://science.sciencemag.org/content/352/6290/1210`.

[15] Zhu, X.-G., Long, S. P. & Ort, D. R. What is the maximum efficiency with which photosynthesis can convert solar energy into biomass? *Current Opinion in Biotechnology* **19**, 153–159 (2008). URL `https://www.sciencedirect.com/science/article/pii/S0958166908000165`.

[16] Zhu, X.-G., Long, S. P. & Ort, D. R. Improving Photosynthetic Efficiency for Greater Yield. *Annual Review of Plant Biology* **61**, 235–261 (2010). URL `http://www.annualreviews.org/doi/10.1146/annurev-arplant-042809-112206`.

[17] Green, M. A. *et al.* Solar cell efficiency tables (Version 53). *Progress in Photovoltaics: Research and Applications* **27**, 3–12 (2019).

[18] Wijffels, R. H. & Barbosa, M. J. An Outlook on Microalgal Biofuels. *Science* **329**, 796–799 (2010). URL `http://www.ncbi.nlm.nih.gov/pubmed/20705853`.

[19] Lu, X. *et al.* Biomass logistics analysis for large scale biofuel production: Case study of loblolly pine and switchgrass. *Bioresource Technology* **183**, 1–9 (2015).

[20] Adesina, O., Anzai, I. A., Avalos, J. L. & Barstow, B. Embracing Biological Solutions to the Sustainable Energy Challenge. *Chem* **2**, 20–51 (2017).

[21] Li, H. *et al.* Integrated Electromicrobial Conversion of CO_2 to Higher Alcohols. *Science* **335**, 1596–1596 (2012).

[22] Lu, J., Brigham, C. J., Gai, C. S. & Sinskey, A. J. Studies on the production of branched-chain alcohols in engineered *Ralstonia eutropha*. *Applied Microbiology and Biotechnology* **96**, 283–297 (2012). URL `https://www.ncbi.nlm.nih.gov/pubmed/22864971`.

[23] Ueki, T. *et al.* Construction of a *Geobacter* Strain With Exceptional Growth on Cathodes. *Frontiers in Microbiology* **9**, 1512 (2018).

[24] Tashiro, Y., Hirano, S., Matson, M. M., Atsumi, S. & Kondo, A. Electrical-biological hybrid system for CO_2 reduction. *Metabolic Engineering* **47**, 211–218 (2018). URL `https://doi.org/10.1016/j.ymben.2018.03.015`.

[25] Grousseau, E., Lu, J., Gorret, N., Guillouet, S. E. & Sinskey, A. J. Isopropanol production with engineered *Cupriavidus necator* as bioproduction platform. *Applied Microbiology and Biotechnology* **98**, 4277–4290 (2014).

[26] Firer-Sherwood, M., Pulcu, G. S. & Elliott, S. J. Electrochemical interrogations of the Mtr cytochromes from *Shewanella*: Opening a potential window. *Journal of Biological Inorganic Chemistry* **13**, 849–854 (2008). URL `https://www.ncbi.nlm.nih.gov/pubmed/18575901`.

[27] Appel, A. M. *et al.* Frontiers, Opportunities, and Challenges in Biochemical and Chemical Catalysis of CO_2 Fixation. *Chemical Reviews* **113**, 6621–6658 (2013). URL `https://pubs.acs.org/doi/10.1021/cr300463y`.

[28] White, J. L., Herb, J. T., Kaczur, J. J., Majsztrik, P. W. & Bocarsly, A. B. Photons to formate: Efficient electrochemical solar energy conversion via reduction of carbon dioxide. *Journal of CO2 Utilization* **7**, 1–5 (2014). URL `http://dx.doi.org/10.1016/j.jcou.2014.05.002`.

[29] White, J. L. *et al.* Light-Driven Heterogeneous Reduction of Carbon Dioxide: Photocatalysts and Photoelectrodes. *Chemical Reviews* **115**, 12888–12935 (2015). URL `https://pubs.acs.org/doi/full/10.1021/acs.chemrev.5b00370`.

[30] Burgdorf, T. *et al.* [NiFe]-Hydrogenases of *Ralstonia eutropha* H16: Modular Enzymes for Oxygen-Tolerant Biological Hydrogen Oxidation. *Journal of Molecular Microbiology and Biotechnology* **10**, 181–196 (2005).

[31] Barstow, B. Molecular Mechanisms for the Biological Storage of Renewable Energy. *Advanced Science, Engineering and Medicine* **7**, 1066–1081 (2015).

[32] Agapakis, C. M. *et al.* Insulation of a synthetic hydrogen metabolism circuit in bacteria. *Journal of Biological Engineering* **4**, 3 (2010).

[33] Barstow, B. *et al.* A synthetic system links FeFe-hydrogenases to essential *E. coli* sulfur metabolism. *Journal of Biological Engineering* **5**, 7 (2011).

[34] Ducat, D. C., Sachdeva, G. & Silver, P. A. Rewiring hydrogenase-dependent redox circuits in cyanobacteria. *Proceedings of the National Academy of Sciences* **108**, 3941–3946 (2011).

[35] Schwander, T., von Borzyskowski, L. S., Burgener, S., Cortina, N. S. & Erb, T. J. A synthetic pathway for the fixation of carbon dioxide *in vitro*. *Science* **354**, 900–904 (2016).

[36] Milo, R., Jorgensen, P., Moran, U., Weber, G. & Springer, M. BioNumbers - the database of key numbers in molecular and cell biology. *Nucleic Acids Research* **38**, D750–D753 (2010).

[37] Esswein, A. J., Surendranath, Y., Reece, S. Y. & Nocera, D. G. Highly active cobalt phosphate and borate based oxygen evolving catalysts operating in neutral and natural waters. *Energy & Environmental Science* **4**, 499–504 (2011).

[38] Chen, A. H., Robinson-Mosher, A., Savage, D. F., Silver, P. A. & Polka, J. K. The Bacterial Carbon-Fixing Organelle Is Formed by Shell Envelopment of Preassembled Cargo. *PLoS ONE* **8**, e76127 (2013).

[39] Polka, J. K. & Silver, P. A. A Tunable Protein Piston That Breaks Membranes to Release Encapsulated Cargo. *ACS Synthetic Biology* **5**, 303–311 (2016).

[40] Butterfield, G. L. *et al.* Evolution of a designed protein assembly encapsulating its own RNA genome. *Nature* **552**, 415 (2017).

[41] Nelson, J. *The Physics of Solar Cells* (Imperial College Press, 2003).

[42] Brigham, C. J. *et al.* Engineering *Ralstonia eutropha* for Production of Isobutanol from CO_2, H_2, and O_2. In Lee, J. W. (ed.) *Advanced Biofuels and Bioproducts*, vol. 1, chap. 39, 1065–1090 (Springer, 2013).

[43] Kenji Tanaka, T. K. T. K., Ayaaki Ishizaki. Production of poly(D-3-hydroxybutyrate) from CO_2, H_2, and O_2 by high cell density autotrophic cultivation of *Alcaligenes eutrophus*. *Biotechnology and Bioengineering* **45**, 268–275 (1995).

[44] Worden, R. M. & Liu, Y. C. Catalytic bioreactors and methods of using same (2017).

[45] Van't Riet, K. Review of Measuring Methods and Results in Nonviscous Gas-Liquid Mass Transfer in Stirred Vessels. *Industrial & Engineering Chemistry Process Design and Development* **18**, 357–364 (1979).

[46] Sydow, A., Krieg, T., Mayer, F., Schrader, J. & Holtmann, D. Electroactive bacteria–molecular mechanisms and genetic tools. *Applied Microbiology and Biotechnology* **98**, 8481–8495 (2014).

[47] Fredrickson, J. K. *et al.* Towards environmental systems biology of *Shewanella*. *Nature Reviews Microbiology* **6**, 592–603 (2008).

[48] Shi, L. *et al.* Molecular Underpinnings of Fe(III) Oxide Reduction by *Shewanella oneidensis* MR-1. *Frontiers in Microbiology* **3**, 50 (2012).

[49] Shi, L. *et al.* Extracellular electron transfer mechanisms between microorganisms and minerals. *Nature Reviews Microbiology* **14**, 651–662 (2016). URL `http://dx.doi.org/10.1038/nrmicro.2016.93`.

[50] Bird, L. J., Bonnefoy, V. & Newman, D. K. Bioenergetic challenges of microbial iron metabolisms. *Trends in Microbiology* **19**, 330–340 (2011). URL `http://dx.doi.org/10.1016/j.tim.2011.05.001`.

[51] Thauer, R. K., Jungermann, K. & Decker, K. Energy Conservation in Chemotrophic Anaerobic Bacteria. *Bacteriological Reviews* **41**, 100–180 (1977).

[52] Liu, J. *et al.* Identification and characterization of M to A: A decaheme c-type cytochrome of the neutrophilic Fe(II)-oxidizing bacterium *Sideroxydans lithotrophicus* ES-1. *Frontiers in Microbiology* **3**, 1–11 (2012).

[53] Bonis, B. M. & Gralnick, J. A. *Marinobacter subterrani*, a genetically tractable neutrophilic Fe(II)- oxidizing strain isolated from the Soudan Iron Mine. *Frontiers in Microbiology* **6**, 1–11 (2015). URL `https://www.ncbi.nlm.nih.gov/pubmed/26236300`.

[54] Canfield, D. E., Rosing, M. T. & Bjerrum, C. Early anaerobic metabolisms. *Philosophical Transactions of the Royal Society B: Biological Sciences* **361**, 1819–1836 (2006). URL `http://rstb.royalsocietypublishing.org/cgi/doi/10.1098/rstb.2006.1906`.

[55] Rowe, A. R. *et al.* Tracking electron uptake from a cathode into *Shewanella* cells: Implications for energy acquisition from solid-substrate electron donors. *mBio* **9**, 1–19 (2018). URL `https://mbio.asm.org/content/9/1/e02203-17`.

[56] Bose, A., Gardel, E. J., Vidoudez, C., Parra, E. A. & Girguis, P. R. Electron uptake by iron-oxidizing phototrophic bacteria. *Nature Communications* **5**, 3391 (2014). URL `http://dx.doi.org/10.1038/ncomms4391`.

[57] Tang, H.-Y., Holmes, D. E., Ueki, T., Palacios, P. A. & Lovley, D. R. Iron Corrosion via Direct Metal-Microbe Electron Transfer. *mBio* **10**, 1–10 (2019). URL `https://mbio.asm.org/content/10/3/e00303-19`.

[58] Zheng, Z. *et al.* Electrons selective uptake of a metal-reducing bacterium *Shewanella oneidensis* MR-1 from ferrocyanide. *Biosensors and Bioelectronics* **142**, 111571 (2019). URL `https://doi.org/10.1016/j.bios.2019.111571`.

[59] Malvankar, N. S., Tuominen, M. T. & Lovley, D. R. Biofilm conductivity is a decisive variable for high-current-density *Geobacter sulfurreducens* microbial fuel cells. *Energy & Environmental Science* **5**, 5790–5797 (2012).

[60] Renslow, R. *et al.* Mathematical modeling of extracellular electron transfer in biofilms. In Beyenal, H. & Babauta, J. (eds.) *Biofilms in Bioelectrochemical Systems*, chap. 9, 281–344 (John Wiley & Sons, Ltd, 2015). URL `https://onlinelibrary.wiley.com/doi/abs/10.1002/9781119097426.ch9`. `https://onlinelibrary.wiley.com/doi/pdf/10.1002/9781119097426.ch9`.

[61] Yates, M. D. *et al.* Thermally activated long range electron transport in living biofilms. *Physical Chemistry Chemical Physics* **17**, 32564–32570 (2015).

[62] El-Naggar, M. Y. *et al.* Electrical transport along bacterial nanowires from *Shewanella oneidensis* MR-1. *Proceedings of the National Academy of Sciences* **107**, 18127–18131 (2010). URL `http://www.pnas.org/cgi/doi/10.1073/pnas.1004880107`.

[63] Meysman, F. J. R. *et al.* A highly conductive fibre network enables centimetre-scale electron transport in multicellular cable bacteria. *Nature Communications* **10**, 4120 (2019).

[64] Polizzi, N. F., Skourtis, S. S. & Beratan, D. N. Physical constraints on charge transport through bacterial nanowires. *Faraday Discussions* **155**, 43–62 (2012). URL `https://www.ncbi.nlm.nih.gov/pubmed/22470966`. `NIHMS150003`.

[65] Siegel, J. B. *et al.* Computational protein design enables a novel one-carbon assimilation pathway. *Proceedings of the National Academy of Sciences* **112**, 201500545 6 (2015).

[66] Bar-Even, A. Formate Assimilation: The Metabolic Architecture of Natural and Synthetic Pathways. *Biochemistry* **55**, 3851–63 (2016).

[67] Antonovsky, N. *et al.* Sugar Synthesis from CO2 in Escherichia coli. *Cell* **166**, 115 125 (2016).

[68] Gleizer, S. *et al.* Conversion of *Escherichia coli* to Generate All Biomass Carbon from CO_2. *Cell* **179**, 1255–1263.e12 (2019).

[69] Beyenal, H. & Babauta, J. *Biofilms in Bioelectrochemical Systems* (John Wiley & Sons, 2015).

[70] Nguyen, P. Q., Botyanszki, Z., Tay, P. K. R. & Joshi, N. S. Programmable biofilm-based materials from engineered curli nanofibres. *Nature communications* **5**, 4945 (2014).

[71] Rowe, S. F. *et al.* Light-Driven H_2-Evolution and C=C or C=O Bond Hydrogenation by *Shewanella oneidensis*: A Versatile Strategy for Photocatalysis by Non-Photosynthetic Microorganisms. *ACS Catalysis* (2017).

[72] Virtanen, P. *et al.* SciPy 1.0–Fundamental Algorithms for Scientific Computing in Python. *arXiv e-prints* arXiv:1907.10121 (2019). 1907.10121.

[73] van der Walt, S., Colbert, S. C. & Varoquaux, G. The NumPy Array: A Structure for Efficient Numerical Computation. *Computing in Science & Engineering* **13**, 22–30 (2010).

[74] Hunter, J. Matplotlib: A 2D Graphics Environment. *Computing in Science & Engineering* **9**, 90–95 (2007).